ACS Synthetic Biology
Research Article
Cite This: ACS Synth. Biol. 2018, 7, 2879−2887
pubs.acs.org/synthbio

Sigma Factor-Mediated Tuning of Bacterial Cell-Free Synthetic Genetic Oscillators

Maaruthy Yelleswarapu,[†,§] Ardjan J. van der Linden,[‡,§] Bob van Sluijs,[†] Pascal A. Pieters,[‡] Emilien Dubuc,[‡] Tom F. A. de Greef,[*,‡] and Wilhelm T. S. Huck[*,†]

[†]Radboud University, Institute for Molecules and Materials, Heyendaalseweg 135, 6525 AJ Nijmegen, The Netherlands
[‡]Institute for Complex Molecular Systems, Department of Biomedical Engineering, Computational Biology Group, Eindhoven University of Technology, P.O. Box 513, 5600 MB Eindhoven, The Netherlands

Supporting Information

ABSTRACT: Cell-free transcription−translation provides a simplified prototyping environment to rapidly design and study synthetic networks. Despite the presence of a well characterized toolbox of genetic elements, examples of genetic networks that exhibit complex temporal behavior are scarce. Here, we present a genetic oscillator implemented in an *E. coli*-based cell-free system under steady-state conditions using microfluidic flow reactors. The oscillator has an activator−repressor motif that utilizes the native transcriptional machinery of *E. coli*: the RNAP and its associated sigma factors. We optimized a kinetic model with experimental data using an evolutionary algorithm to quantify the key regulatory model parameters. The functional modulation of the RNAP was investigated by coupling two oscillators driven by competing sigma factors, allowing the modification of network properties by means of passive transcriptional regulation.

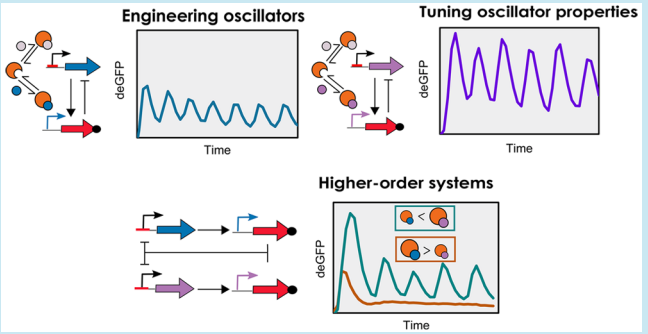

KEYWORDS: *oscillator, cell-free systems, synthetic biology, sigma factors, competition-induced regulation*

Synthetic biology employs synthetic genetic networks to re-engineer organisms for a range of applications. Synthetic genetic circuits have been designed to display higher-order temporal functions,[1−4] perform logic operations in cells,[5,6] and produce heterologous proteins in microorganisms.[7−10] A major difficulty faced by synthetic biology concerns the implementation of synthetic genetic networks in living organisms, which presents an unnatural load for the host organism and affects the cell growth, often leading to the poor performance of engineered circuits.[11]

Cell-free protein synthesis (TX-TL) has the potential to serve as a biochemical breadboard that allows for the rapid prototyping of genetic networks without interference from cellular hosts.[12,13] Numerous works have focused on the optimization of protein expression from bacterial cell-free systems,[14−18] which has resulted in a well-characterized toolbox of genetic elements comprising a range of transcriptional and translational regulators.[19−21] This toolbox extends the variety of synthetic genetic networks that can be constructed by allowing the use of essential bacterial machinery that would be difficult to achieve *in vivo* (*E. coli*), as they are important to the native functionality of the cell. Synthetic cascades, which use transcriptional machinery such as the T7 RNA polymerase (RNAP) and bacterial RNAP, have been engineered using this cell-free toolbox.[19,20,22] Since such circuits exhibit linear behavior, they can be prototyped in batch TX-TL conditions, as their functioning does not depend on the balance of rates between the individual steps. To engineer networks that exhibit complex behavior—such as oscillations—batch conditions are insufficient primarily because the resources available for the synthesis of mRNAs and proteins are finite and the utilization of these resources results in byproducts that can inhibit critical TX-TL components.[20] To extend the lifetime of TX-TL reactions, microfluidic platforms have been designed wherein the TX-TL components can be replenished, thereby creating an open system wherein the transcription and translation rates are sustained in a steady state.

Karzbrun *et al.* studied oscillatory behavior in continuous TX-TL reactions by immobilizing DNA networks within two-dimensional microfluidic compartments. Separated from the central flow channel, their system relied on the diffusion of TX-TL reagents components through capillary channels to reach the DNA compartments, enabling the dynamics of a cell-free oscillator to be tuned by changing the dimensions thereof.[23] Niederholtmeyer *et al.* utilized pneumatically controlled microfluidic flow reactors to study numerous ring oscillators under steady-state TX-TL conditions, showing that the qualitative and quantitative performance of the oscillators *in vitro* reflect those in *in vivo* conditions.[24]

Received: July 13, 2018
Published: November 8, 2018

DOI: 10.1021/acssynbio.8b00300
ACS Synth. Biol. 2018, 7, 2879−2887

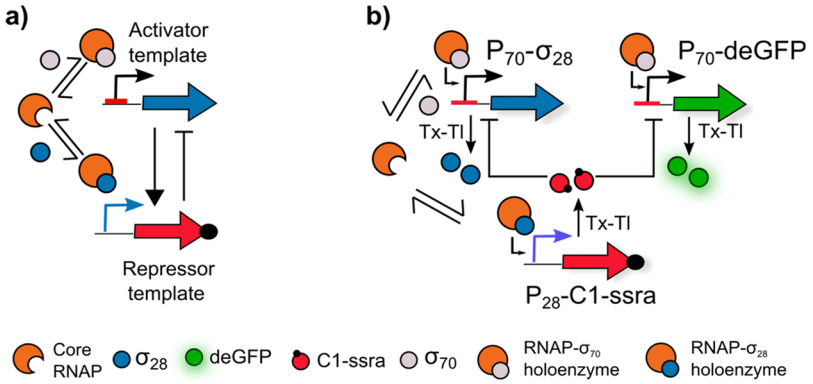

Figure 1. (a) The oscillator has an activator−repressor motif with the σ_{28} and C1 serving as activator and repressor, respectively. Critical to the functioning of the oscillator is the competitive binding between the two sigma factors to the core RNAP to form their respective holoenzymes. (b) Schematic representation of the σ_{28}-oscillator. The network topology comprises three DNA constructs: **P_{70}-σ_{28}**, **P_{28}-C1-ssra**, and **P_{70}-deGFP**. The σ_{70} binds to the RNAP to form the RNAP-σ_{70} holoenzyme, which binds to the P_{70} promoter and initiates the expression of σ_{28} and deGFP. σ_{28} competitively binds to RNAP to form the RNAP-σ_{28} holoenzyme, which binds to the P_{28} promoter and initiates the expression of C1-ssra. C1-ssra exclusively binds to the P_{70} promoter and represses the production of σ_{28} and deGFP.

Despite the availability of a well characterized cell-free toolbox and long-lived TX-TL platforms, the full repertoire of available elements has not been used to engineer higher-order genetic networks. In order to expand the toolbox, it is necessary to implement the toolbox elements to design complex genetic networks, such as oscillators, in open systems where key TX-TL resources are not limiting. Oscillatory networks are important as they control key aspects of life such as circadian rhythms, cell division, metabolism and cell signaling.[25] However, engineering oscillators is challenging because their design requires an optimal balance of rates of the various regulatory processes involved.[26] To aid the systematic engineering of oscillators, mathematical models can be used to provide a mechanistic understanding of the system and facilitate the design of higher-order network topologies.[24] In our research, we focused on engineering a synthetic genetic oscillator in an open TX-TL system, leveraging an important regulatory component of *E. coli* machinery: the endogenous RNAP and its associated sigma factors. Bacterial RNAP is a multisubunit enzyme that uses sigma factors to help in transcription initiation.[27] Despite the regulatory role of sigma factors *in vivo* being well understood,[28−30] their potential in engineering complex genetic networks is only starting to be realized. Recently it has been shown that bacteria use sigma factors to alter the transcriptional landscape under stressed conditions by time-sharing the core RNAP, thereby modulating its function.[31] Bervoets *et al.* have recently engineered a sigma factor toolbox belonging to *B. subtilis* as an orthogonal transcriptional control mechanism that can be used in other bacterial species such as *E. coli*.[32] Karzbrun *et al.* and Tayar *et al.* have implemented sigma-factor based oscillators in TX-TL systems to demonstrate the emergence of collective behavior such as entrainment and synchronization between coupled oscillators.[23,33] Since sigma factors allow convenient reprogramming of the transcriptional machinery and exhibit versatile properties with respect to binding to RNAP and DNA, using them as regulatory molecules in oscillators will improve our ability to modulate systems-level behavior of genetic networks. Furthermore, the competition of sigma factors for the core RNAP allows for the facile coupling of multiple networks driven by different sigma factors and thereby enables the engineering of synthetic genetic networks displaying higher-order regulatory functions.

Here, we present the characterization of a two-component oscillator with an activator−repressor motif and a delayed negative feedback topology based on genetic elements from the *E. coli* cell-free Toolbox 2.0.[20] Our initial network (Figure 1) is based on the sigma factor 28 (σ_{28}) serving as the activator, the C1 protein serving as a repressor, and deGFP as a reporter. We have quantitatively characterized every genetic element as well as the behavior of the network, by optimizing a mathematical model with experimental data using an evolutionary algorithm. This has enabled us to map the characteristics and behavior of this oscillator. Subsequently we replaced σ_{28} with sigma factor 19 (σ_{19}) to modify the oscillatory regime of the network and proceeded to investigate the influence of competition-driven passive transcriptional control between sigma factors on network behavior by coupling the two oscillators. All oscillators were characterized experimentally in a *E. coli*-based TX-TL system operating under steady-state conditions in microfluidic flow reactors.[12]

RESULTS AND DISCUSSION

Bottom-Up Engineering of the σ_{28}-Oscillator. The oscillator presented here is based on a delayed negative feedback topology (Figure 1a) as introduced by Stricker *et al.*[4] The oscillatory network constitutes an activator−repressor motif, as also found in several natural systems,[34] and utilizes the σ_{28} as an activator and the C1 protein as the repressor (Figure 1b). In contrast to previous works, which have been performed in diffusion-limited TX-TL environments,[23,33] we have implemented this design under well-mixed conditions in order to study fundamental mechanisms in the system such as the asymmetric competition between sigma factors for core RNAP. This asymmetric competition determines the amount of holoenzyme of each sigma factor—the complex formed by the association of sigma factor and RNAP—available to transcribe genes from their respective promoters.[19,29] Furthermore, the sharing of critical catalytic resources, such as RNAP, in biochemical circuits plays an important role in affecting network behavior.

The oscillatory network comprises three DNA constructs: **P_{70}-σ_{28}**, **P_{28}-C1-ssra**, and **P_{70}-deGFP** (Figure 1b). The

DOI: 10.1021/acssynbio.8b00300
ACS Synth. Biol. 2018, 7, 2879−2887

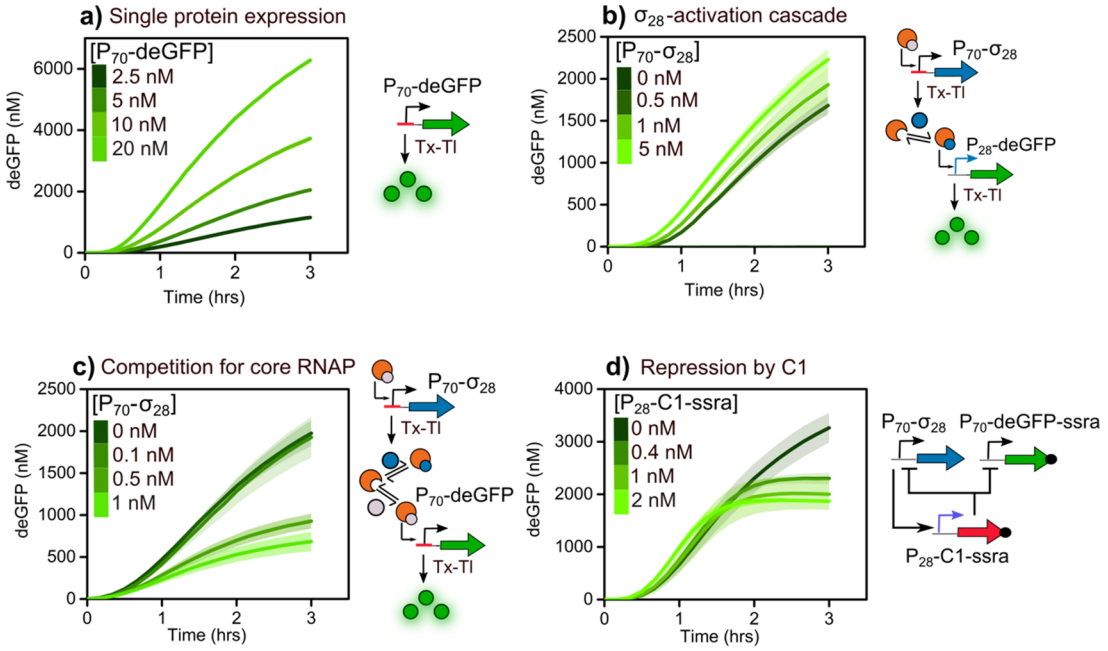

Figure 2. Time traces of deGFP production as readout for the key regulatory mechanisms of the σ_{28}-oscillator under batch TX-TL conditions. (a) Linear DNA template (**P_{70}-deGFP**) at different concentrations. (b) Two-step σ_{28}-activation cascade. Increasing concentrations of **P_{70}-σ_{28}** template were added to 5 nM of **P_{28}-deGFP** template. Expression of σ_{28} from **P_{70}-σ_{28}** activates deGFP production. (c) Expression from **P_{70}-deGFP** under competition for core RNAP between sigma factors σ_{70} and σ_{28}. Increasing concentrations of **P_{70}-σ_{28}** template were added to 5 nM of **P_{70}-deGFP**. (d) Transcriptional repression by C1. The concentrations of **P_{70}-deGFP-ssra** and **P_{70}-σ_{28}** were fixed at 5 and 0.1 nM, respectively, to which increasing concentrations of **P_{28}-C1-ssra** template were added. Shaded error bands are standard error of three separate measurements.

expression of σ_{28} is regulated by the P_{70} promoter. Transcription from this promoter is initiated when sigma factor 70 (σ_{70}) binds to the core bacterial RNAP to form the RNAP-σ_{70} holoenzyme, which can subsequently bind to the P_{70} promoter. Once expressed, the σ_{28} protein binds competitively to the core RNAP to form the RNAP-σ_{28} holoenzyme and activates expression of genes under control of the P_{28} promoter. This promoter regulates the production of the λ phage protein C1, which binds exclusively at the P_{70} promoter, thereby inhibiting the transcription and the eventual production of σ_{28}. Additionally, the C1 protein contains a C-terminal ssra tag for targeted protein degradation by ClpXP proteases. These proteases, along with the σ_{70}, bacterial RNAP, and the necessary translational machinery (ribosomes, elongation factors, *etc.*) are present in the *E. coli* cell lysate.[16] Finally a reporter protein, deGFP[19,29]—also under the control of P_{70} promoter—is incorporated as a fluorescent readout.

Since designing oscillators is a challenging process and involves a fine balance of rates among regulatory components, we implemented an ordinary differential equation (ODE)-based mathematical model to quantify our system and inform our experiments. We described the network using a kinetic model (SI, eq 1.1−1.11) that takes into consideration the four key processes: (i) transcription and translation of each DNA construct, (ii) competition between σ_{28} and σ_{70} for RNAP, (iii) repression by the C1 protein, and (iv) dilution (under steady-state TX-TL conditions) and degradation of mRNA and protein species. Having determined an upper and lower boundary for each model parameter based on literature, we sampled the parameter space using Latin Hypercube Sampling (LHS) to test if this motif yielded oscillatory dynamics under steady-state TX-TL conditions (Figure S1). The analysis revealed that 29% of the sampled parameter sets showed oscillations, indicating that the motif is robust in its ability to oscillate (Figure S1a).

In order to identify individual parameters in our model,[35] the key regulatory mechanisms of our network were implemented separately under batch TX-TL conditions (Figure 2). First, we added increasing concentrations of the **P_{70}-deGFP** template to the TX-TL reaction mix (Figure 2a). We observed an increased expression of deGFP upon increasing template concentration confirming the presence of σ_{70} in the lysate. Next, we implemented a two-step cascade to test transcriptional activation by σ_{28} (Figure 2b) by adding increasing amounts of **P_{70}-σ_{28}** template to a fixed concentration of **P_{28}-deGFP** template. No deGFP fluorescence was observed in the absence of the **P_{70}-σ_{28}** template indicating the absence of σ_{28} in the lysate. We observed deGFP fluorescence upon addition of 0.5 nM of **P_{70}-σ_{28}** template indicating the production of functional σ_{28}, which activates protein production from the P_{28} promoter. The onset of deGFP expression and the final yield did not improve remarkably upon increasing the **P_{70}-σ_{28}** template concentration from 0.5 to 5 nM, highlighting the potency of σ_{28} as a transcriptional activator. Since the design of the network involves two sigma factors competing for the RNAP, we quantified the extent of this competition by adding increasing amounts of **P_{70}-σ_{28}** template to a fixed concentration of **P_{70}-deGFP** template (Figure 2c). The sequestration of core RNAP by σ_{28} and the subsequent decrease in deGFP expression serves as an indirect measurement for sigma factor competition. We observed that the addition of 0.5 nM of the **P_{70}-σ_{28}** template is enough to produce sufficient σ_{28} to outcompete σ_{70} for the core RNAP, reducing the deGFP yield by approximately 50% when compared to the control (without any **P_{70}-σ_{28}** template). To verify that this decrease resulted from competition between sigma factors and not from depletion of TX-TL resources, we

DOI: 10.1021/acssynbio.8b00300
ACS Synth. Biol. 2018, 7, 2879−2887

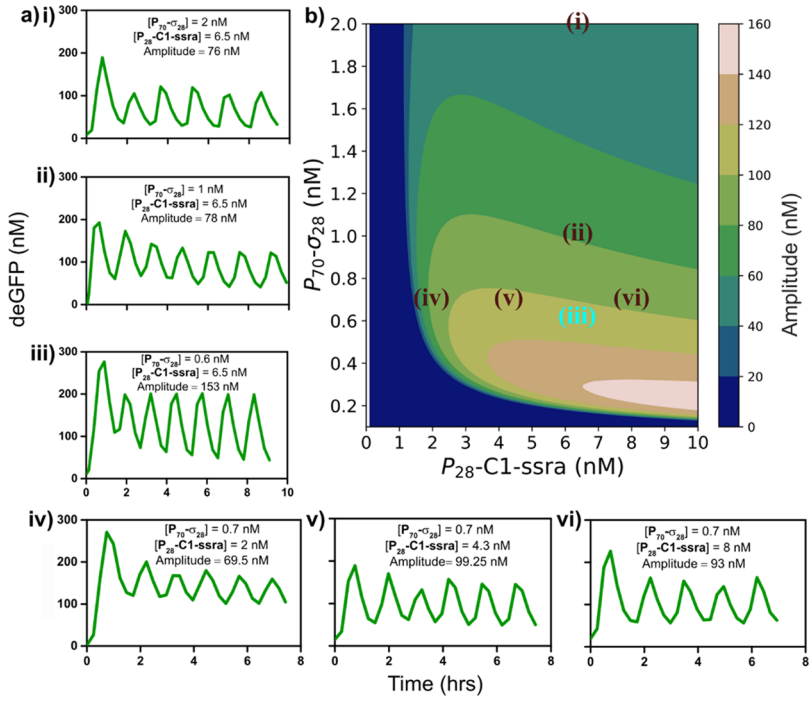

Figure 3. Characterization of the σ_{28}-oscillator. (a) (i–vi) Experimentally obtained deGFP time courses for the σ_{28}-oscillator exhibiting sustained oscillations under steady-state TX-TL conditions for various values of [$\mathbf{P_{70}}$-$\boldsymbol{\sigma_{28}}$, $\mathbf{P_{28}}$-**C1-ssra**]. (b) Contour plot showing the model-predicted amplitude of oscillations mapped on to [$\mathbf{P_{70}}$-$\boldsymbol{\sigma_{28}}$, $\mathbf{P_{28}}$-**C1-ssra**] phase space for a given refresh rate (0.026 min^{-1}). All points in a(i–vi) have been mapped on to the contour plot in (b). Since a(iii) was used to re-estimate model parameters and obtain the contour plot, it has been shown in blue. $\mathbf{P_{70}}$-**deGFP** template concentration and refresh rate were fixed at 8 nM and 0.026 min^{-1}, respectively, in all experiments.

repeated the same experiment using the $\mathbf{P_{70}}$-$\boldsymbol{\sigma_{19}}$ template instead of the $\mathbf{P_{70}}$-$\boldsymbol{\sigma_{28}}$ template (Figure S2a). The addition of 1 nM of the $\mathbf{P_{70}}$-$\boldsymbol{\sigma_{19}}$ template did not result in any significant reduction in the expression of the deGFP, indicating that the previously noted decrease is indeed caused by the competition of σ_{28} with σ_{70} for the core RNAP and is not the result of depletion of resources. The final regulatory mechanism tested is the transcriptional repression by C1 (Figure 2d). We fixed the concentration of $\mathbf{P_{70}}$-**deGFP-ssra** template at 5 nM and $\mathbf{P_{70}}$-$\boldsymbol{\sigma_{28}}$ template at 0.1 nM, thus ensuring that any decrease in the expression yield of deGFP is the result of inhibition *via* the C1 protein as opposed to competition from σ_{28}, and added increasing concentrations of $\mathbf{P_{28}}$-**C1-ssra** template. We observed that the C1 protein inhibits protein production from the P_{70} promoter, thereby decreasing the yields of deGFP for concentrations of $\mathbf{P_{28}}$-**C1-ssra** template as low as 0.4 nM.

Since the lifetime of reactions in batch TX-TL conditions is limited, we used the initial expression kinetics to provide us with estimates of reaction rates and binding constants. We implemented an evolutionary algorithm (Figure S3) adapted from Smith *et al.*[36] to evolve model parameters to fit the batch TX-TL data (Figure S4). Using this initial parameter (Table S1) set we predicted an oscillatory regime for our network described by three experimentally controlled parameters—$\mathbf{P_{70}}$-$\boldsymbol{\sigma_{28}}$ template concentration, $\mathbf{P_{28}}$-**C1-ssra** template concentration, and refresh rate (*vide infra*)—with experimentally feasible upper and lower boundaries for each parameter, which guided our initial experiments in steady-state TX-TL conditions (Figure S5).

Steady-state TX-TL experiments were conducted in a PDMS-based, pneumatically controlled, bilayer microfluidic chip.[12] Each chip comprises eight independent, 11 nL, ring reactors in which unique TX-TL reactions can be performed. The periodic inflow of fresh TX-TL reaction solutions and the simultaneous outflow of used reagents allows the system to operate such that the transcription and translation rates are in steady state and extends the lifetime of TX-TL reactions. The period between subsequent dilutions (injection of fresh reagents into reactor while removing used reagents) and the volume fraction of the reactor being replenished per dilution is represented by the refresh rate (Table S3).

Variation of the control parameters regulates the transition of the network through three qualitatively different outputs: sustained oscillations, damped oscillations, and single-peak behavior under steady-state TX-TL conditions (Figure 3a(i–vi) and Figure S6). While the period of oscillations varied marginally (between 74 and 88 min), the amplitude of the oscillations showed significant variations, with the largest oscillation amplitude being observed at $\mathbf{P_{70}}$-$\boldsymbol{\sigma_{28}}$ and $\mathbf{P_{28}}$-**C1-ssra** concentrations of 0.6 and 6.5 nM, with a refresh rate of 0.026 min^{-1} (Figure 3a(iii)). Lowering the refresh rate for comparable concentrations of $\mathbf{P_{70}}$-$\boldsymbol{\sigma_{28}}$ and $\mathbf{P_{28}}$-**C1-ssra** templates resulted in the dampening of oscillations (Figure S6a). Increasing the concentration of $\mathbf{P_{28}}$-**C1-ssra** template, for a fixed $\mathbf{P_{70}}$-$\boldsymbol{\sigma_{28}}$ concentration and refresh rate, increased the amplitude of damped oscillations (Figure S6b,c). These results indicate that since σ_{28} is a transcriptionally strong sigma factor (Figure 2b) it produces C1 protein rapidly and the refresh rate needs to be sufficiently high to remove σ_{28} thereby generating the sufficient time delay for the negative feedback needed to observe oscillations. These results are in general agreement with our LHS analysis and previous work on similar systems.[33] Increasing the concentrations of the $\mathbf{P_{70}}$-$\boldsymbol{\sigma_{28}}$ and $\mathbf{P_{28}}$-**C1-ssra** templates to 3 and 10 nM, respectively, results in a loss of oscillations and leads to a single transient peak (Figure S6e,f).

DOI: 10.1021/acssynbio.8b00300
ACS Synth. Biol. 2018, 7, 2879–2887

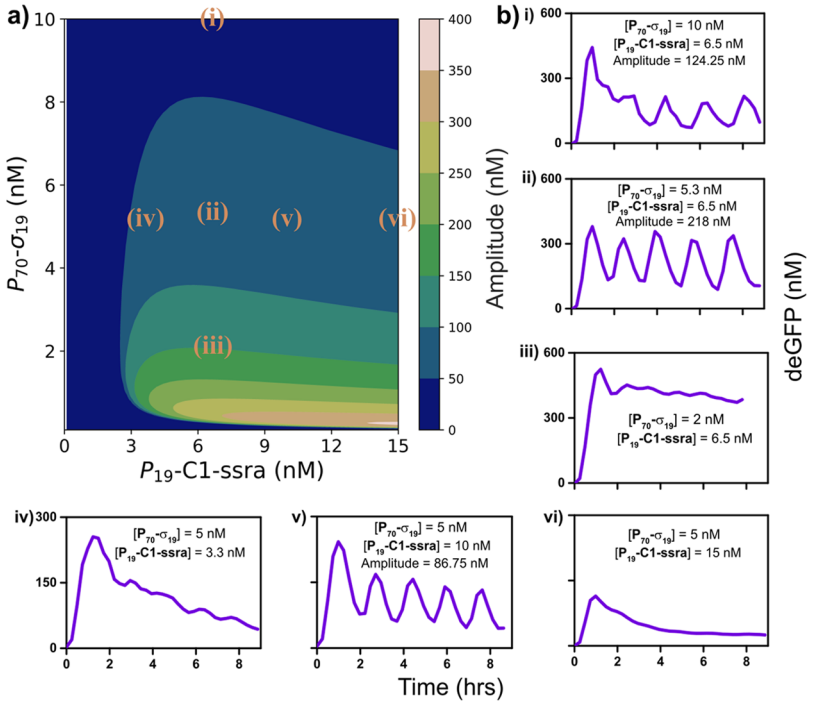

Figure 4. Characterization of the σ_{19}-oscillator. (a) Contour plot showing the model-predicted oscillation amplitudes mapped on to the [**P_{70}-σ_{19}**,**P_{19}-C1-ssra**] phase space for a given refresh rate (0.026 min^{-1}). (b) (i–vi) Experimentally obtained deGFP time courses for the σ_{19}-oscillator exhibiting oscillatory and non-oscillatory behavior for various values of [**P_{70}-σ_{19}**, **P_{19}-C1-ssra**]. All points have been mapped on to the contour plot (a). **P_{70}-deGFP** template concentration and refresh rate were fixed at 8 nM and 0.026 min^{-1}, respectively, in all experiments.

Characterization and Modification of Oscillator Properties. Although our initial parameter estimates from batch TX-TL data aided in finding an oscillatory regime, they did not fully capture the dynamics of the oscillator completely. To improve the accuracy of our model parameters, we re-estimated them by fitting the model to the steady-state TX-TL data using a data point within (Figure 3a(iii)) and outside (Figure S6f) the oscillating regime (Figure S7, Table S1). Using this optimized parameter set we characterized the behavior of the σ_{28}-oscillator by simulating a control parameter space consisting of 15,625 combinations of the control parameters and estimated the subset of this control parameter space for which the model predicts stable oscillations (Figure S8a). The amplitude of oscillations, as predicted by the model, were plotted against the **P_{70}-σ_{28}** and **P_{28}-C1-ssra** template concentrations for a fixed refresh rate (0.026 min^{-1}) (Figure 3b). In order to test the predictive ability of the model, we compared the predicted and observed oscillation amplitudes for the sustained oscillations in Figure 3a. We found that the model predicts a decrease in amplitude of oscillations with increasing **P_{70}-σ_{28}** template concentrations, for a constant **P_{28}-C1-ssra** template concentration (Figure 3b). Upon increasing the concentration of **P_{70}-σ_{28}** template in the experiments from 1 to 2 nM (Figure 3a(ii) and (i)), for a **P_{28}-C1-ssra** concentration of 6.5 nM, we observed a decrease in the amplitude of oscillations (78 and 76 nM), although the extent of decrease was much less compared to the model prediction. Furthermore, the model predicts that increasing the **P_{28}-C1-ssra** template concentration, for a fixed concentration of **P_{70}-σ_{28}** template, from 2 to 4.3 nM should lead to an increase in oscillation amplitude and upon increasing the concentration further to 8 nM should marginally decrease the oscillation amplitudes. Upon experimental verification, we observed a similar trend (Figure 3a(iv,v,vi)) wherein the amplitude increases from 69.5 nM (**P_{28}-C1-ssra** = 2 nM) to 99.25 nM (**P_{28}-C1-ssra** = 4.3 nM) and then decreases marginally to 93 nM (**P_{28}-C1-ssra** = 8 nM).

A sensitivity analysis was performed to assess the impact of changing a single system parameter on the oscillation amplitude and size of the oscillating regime (Figure S9 and S10). The analysis indicated that decreasing the competitive strength of the activator to the RNAP as a possible modification to increase the size of the oscillatory regime and the robustness of oscillations. Since the *E. coli* transcriptional machinery is composed of a variety of sigma factors, each with different affinities for the core RNAP, we replaced σ_{28} with σ_{19} as the activator. σ_{19} has been reported to be transcriptionally less potent and a weaker competitor for RNAP when compared to σ_{28},[20] which we confirmed in batch TX-TL experiments (Figure S2). In order to compare the behavior of the two oscillators we repeated the simulations from Figures S8a and 3b by assuming a lower value for σ_{19} binding and accounting for increased expression dynamics that was observed in the new TX-TL mixture batch.[37] Herein, it was found that the model predicts a larger oscillatory subset, in particular a broader activator template concentration range, when using σ_{19} as the activator in the network (Figure S11a). When characterizing the behavior of the σ_{19} oscillator in a phase space with a fixed refresh rate (0.026 min^{-1}) (Figure 4a), we found that it indeed exhibited oscillations for a higher range of **P_{70}-σ_{19}** template concentrations (from 5 to 10 nM) compared to the σ_{28}-oscillator (from 0.6 to 2 nM) (Figure 4b(i–ii) and Figure 3). However, the model fails to accurately capture the **P_{70}-σ_{19}** template concentration range for which the network exhibits oscillations, as it also predicts oscillations for the conditions in Figure 4b(iii). Variation of the **P_{19}-C1-ssra** template concentration, while fixing the **P_{70}-σ_{19}** template concentration at 5 nM, yielded sustained oscillations for a

DOI: 10.1021/acssynbio.8b00300
ACS Synth. Biol. 2018, 7, 2879–2887

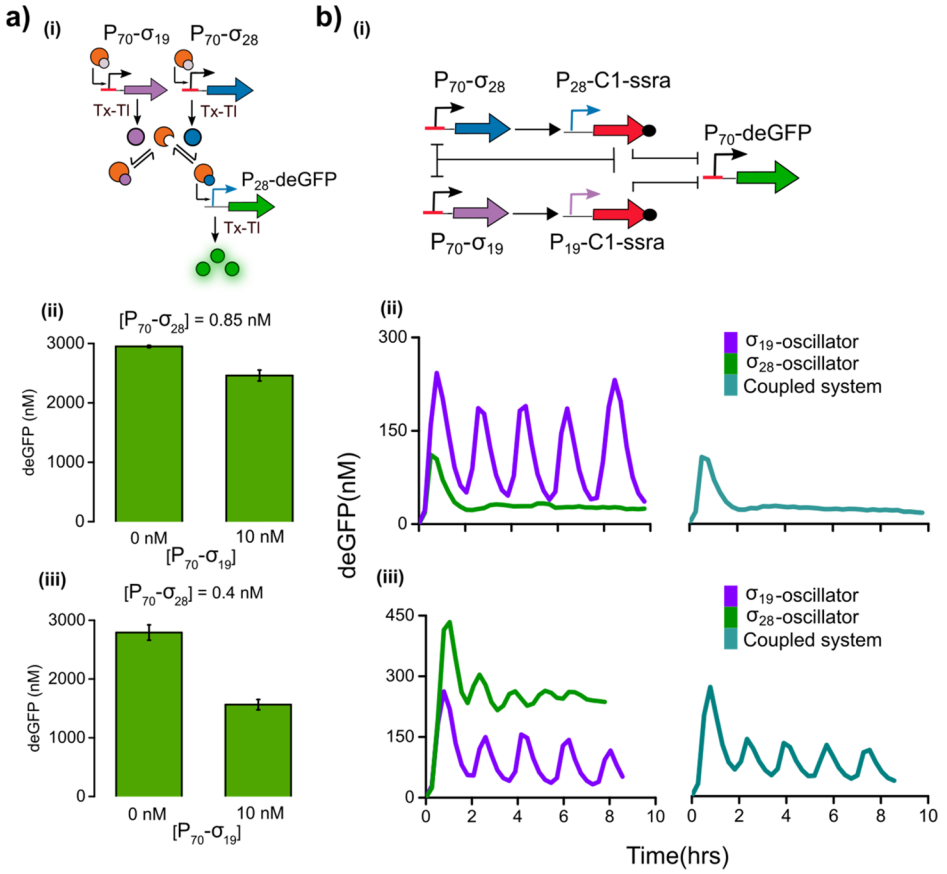

Figure 5. (a) (i) Schematic diagram showing the passive transcriptional regulation exerted by σ_{19} on the σ_{28} activation cascade resulting in the decrease of the deGFP yield due to competition for RNAP by σ_{19}. (ii, iii) End-point measurement of deGFP yields for the batch TX-TL reactions shown for two different concentrations of $\mathbf{P_{70}}$-$\boldsymbol{\sigma_{28}}$: 0.85 and 0.4 nM, respectively. The concentration of $\mathbf{P_{28}}$-**deGFP** DNA template was fixed at 5 nM, and the concentration of $\mathbf{P_{70}}$-$\boldsymbol{\sigma_{19}}$ was varied between 0 and 10 nM. (b) (i) Schematic of the coupled oscillatory network. σ_{19} and σ_{28} regulate the expression of the C1 protein that inhibits the expression of both sigma factors and deGFP. (ii, iii) Experimentally obtained deGFP time traces of the σ_{28}-oscillator, σ_{19}-oscillator, and the coupled system under steady-state TX-TL conditions. The concentration of $\mathbf{P_{70}}$-**deGFP**, $\mathbf{P_{19}}$-**C1-ssra**, and $\mathbf{P_{70}}$-$\boldsymbol{\sigma_{19}}$ were kept fixed at 8, 6.5, and 10 nM, respectively. The respective concentrations of $\mathbf{P_{70}}$-$\boldsymbol{\sigma_{28}}$ and $\mathbf{P_{28}}$-**C1-ssra** were (ii) 0.85 and 6.5 nM and (iii) 0.4 and 1.5 nM.

concentration of 10 nM, while at 3.3 and 15 nM the system does not display any oscillations despite model predictions indicating otherwise (Figure 4b(iv–vi)).

Effect of Passive Transcriptional Control on a Coupled Oscillator. As mentioned above, multiple sigma factors compete for the same pool of core RNAP, and thus an increase in activity of one sigma factor can exert an indirect repression on the binding of another sigma factor to the RNAP.[38] This mechanism is referred to as passive transcriptional regulation.[19] Although present between σ_{28}/σ_{19} and σ_{70} in the individual oscillators, this effect is difficult to investigate as the concentration of σ_{70} is fixed in the lysate. To investigate the extent of such competition-induced regulation among σ_{28} and σ_{19}, we allowed the sigma factors to directly compete for the core RNAP in batch TX-TL, as shown in Figure 5a(i). Comparing deGFP fluorescence in the absence or presence of 10 nM $\mathbf{P_{70}}$-$\boldsymbol{\sigma_{19}}$, we observed that with 0.85 nM of $\mathbf{P_{70}}$-$\boldsymbol{\sigma_{28}}$ template, the σ_{19} only marginally decreases deGFP yield (Figure 5a(ii)). In contrast, lowering the concentration of $\mathbf{P_{70}}$-$\boldsymbol{\sigma_{28}}$ template from 0.85 to 0.4 nM resulted in a decrease of approximately 40% in yield of deGFP due to passive transcriptional repression on the σ_{28}-activation cascade by σ_{19} (Figure 5a(iii)).

In genetic networks, competition for common catalytic resources has been shown to alter network dynamics.[39,40] Coupling the two oscillators within the same network, allows σ_{19} and σ_{28} to drive their respective networks while simultaneously competing for core RNAP. Both sigma factors produce C1 protein that represses the expression of σ_{19}, σ_{28}, and deGFP from their respective templates (Figure 5b(i)). Although multiple factors govern the behavior of such a system, a crucial factor is the competition-induced transcriptional regulation between σ_{28} and σ_{19}. Under steady-state TX-TL conditions, we observed that for a concentration of 0.85 nM of $\mathbf{P_{70}}$-$\boldsymbol{\sigma_{28}}$ the σ_{28}-oscillator displayed a single-peak behavior and at 10 nM of $\mathbf{P_{70}}$-$\boldsymbol{\sigma_{19}}$ the σ_{19}-oscillator showed sustained oscillations. Upon coupling the networks, we found that the system exhibited single-peak behavior (Figure 5b(ii)). However, by decreasing the concentration of the $\mathbf{P_{70}}$-$\boldsymbol{\sigma_{28}}$ to 0.4 nM we found that the σ_{28}-oscillator exhibited damped oscillations and the coupled system showed sustained oscillations (Figure 5b(iii)). This result indicates that decreasing the $\mathbf{P_{70}}$-$\boldsymbol{\sigma_{28}}$ concentration from 0.85 to 0.4 nM allows the system to enter a regime where σ_{19} can better compete for the core RNAP, thereby exerting greater passive transcriptional control over σ_{28}, leading to the emergence of sustained oscillatory behavior in the coupled system. To ensure

DOI: 10.1021/acssynbio.8b00300
ACS Synth. Biol. 2018, 7, 2879–2887

that the preservation of oscillations in the coupled system results from the coupling of oscillators and is not a consequence of extraneous factors such as pressure fluctuations within the microfluidic setup, we coupled the oscillators under conditions for which the isolated σ_{28}-oscillator exhibited no oscillations—sustained or damped—while the σ_{19}-oscillator exhibited sustained oscillations (Figure S12). The concentrations of the $\mathbf{P_{70}}$-$\boldsymbol{\sigma_{28}}$ and $\mathbf{P_{70}}$-$\boldsymbol{\sigma_{19}}$ templates were identical to those used in the experiments depicted in Figure 5b(iii), *i.e.*, 0.4 and 10 nM respectively. We found that the coupled system exhibited sustained oscillations confirming that the behavior of the coupled system is caused by the passive transcriptional control exerted by σ_{19} over σ_{28}.

CONCLUSION

In this work we have implemented cell-free genetic oscillators with an activator−repressor motif leveraging endogenous *E. coli* RNAP and sigma factors. Using an evolutionary algorithm, we optimized a kinetic model with batch and steady-state TX-TL data to characterize a phase space wherein the network exhibits oscillations. Since the sigma factors of both oscillators presented here share a common catalytic resource—RNAP—we were able to observe the behavior of two individual oscillators as well as the behavior of a coupled network wherein both oscillators compete for a common resource. Higher-order systems in synthetic biology are frequently engineered by combining multiple modules downstream of one another, analogous to electrical circuits.[41] In our work, we rely on the RNAP to combine and thereby couple oscillators driven by different sigma factors. We found that the behavior of the coupled oscillator system depends on the extent of passive transcriptional regulation between sigma factors. Together with better understanding of the role of resource sharing[42] and more robust routes to measure kinetic parameters of networks,[43] our study describes a methodology to engineer complex *in vitro* genetic networks.

METHODS

Preparation of DNA Templates. PCR for linear DNA templates was performed using Phusion High-Fidelity DNA Polymerase from ThermoFisher Scientific. PCR was carried out in a thermocycler according to the manufacturer's protocol. DNA templates were purified using QIAGEN PCR purification kits, and concentrations were measured using a Nanodrop. $\mathbf{P_{19}}$-**C1-ssra** template was ordered from IDT as a gBlock fragment. All other DNA templates for this study were obtained from Arbor Biosciences.

Preparation of Cell Lysate. The energy mixture and cell lysate were prepared using protocols described previously by Sun *et al.*[37] and Caschera *et al.*[15] Briefly, BL21 Rosetta2 cells were grown to an OD_{600} of 1.8 in LB medium supplemented with a phosphate buffer (0.22 M sodium dihydrogen phosphate and 0.4 M disodium hydrogen phosphate, pH 7). The cells were washed with S30A buffer (14 mM magnesium glutamate, 60 mM potassium glutamate, 2 mM DTT, titrated to pH 8.2 with Tris-base). The pellet was resuspended in S30A buffer in a volume equal to 0.8 times the cell pellet weight and passed through a cell press at 16 000 lb. The extract was spun down from which the supernatant was collected, incubated at 37 °C, dialyzed in S30B buffer (14 mM magnesium glutamate, 150 mM potassium glutamate, 1 mM DTT, titrated to pH 8.2 with Tris-base) and aliquoted. The density of the cell lysate was determined to be 40 mg/mL using the Pierce BCA assay.

TX-TL Reaction Set Up. The Energy Mixture was added to the cell lysate along with 3 μM GamS, 3% w/v PEG-8000, 6 mM magnesium Glutamate and 80 mM potassium Glutamate to obtain the TX-TL reaction mixture. The final concentrations were 11 mg/mL cell lysate, 50 mM Hepes (pH 8.0), 0.9 mM cytidine triphosphate and uridine triphosphate, 1.5 mM each of adenosine triphosphate and guanosine triphosphate, 0.5 mM of each amino acid, 1 mM spermidine, 0.75 mM cyclic adenosine monophosphate, 0.33 mM nicotinamide adenine dinucleotide, 0.26 mM coenzyme A, 30 mM 3-phosphoglyceric acid, 0.067 mM folinic acid, 0.2 mg/mL tRNAs. For batch TX-TL reactions the DNA templates and necessary volume of MQ H_2O were added and mixed well. Ten μL of the final reaction solution was pipetted into a Nunclon 384 well plate and the deGFP fluorescence was measured using a Tecan M200 Infinite Plate-reader. GamS was prepared using protocols described previously by Sun *et al.*[13]

During the steady-state TX-TL experiments, microfluidic devices were placed within an incubator set to 30 °C. The TX-TL reaction mixture, was stored within a water-cooled Peltier element, maintained at 4 °C. A short piece of tubing was used to connect the Peltier element to the microfluidic device allowing for the injection of the cooled TX-TL mix into the device. The remaining reaction components (*i.e.*, MQ H_2O and DNA solutions) were stored in Tygon tubing (0.02″ ID, 0.06″ OD) that was inserted directly into the microfluidic device. These solutions were maintained at 30 °C for the entirety of the experiment. Over the course of the experiments, fluorescence images were periodically captured using an inverted microscope (Nikon Eclipse) to monitor the fluorescence within the microfluidic reactors. Fluorescence was determined from the obtained images using MATLAB software. Amplitude of sustained oscillations were determined by measuring the difference between the fluorescence maxima and minima of the final two oscillations in the steady-state TX-TL experiments.

Fabrication and Design of Microfluidic device. The microfluidic devices used throughout this research were based on designs published by Niederholtmeyer *et al.*,[12] and were manufactured according to previously described protocols. For more details refer to the Supporting Information.

ASSOCIATED CONTENT

Supporting Information

The Supporting Information is available free of charge on the ACS Publications website at DOI: 10.1021/acssynbio.8b00300.

Model used in the work (SI eq 1.1−1.11); Figures S1−S21; Tables S1−S3; Note on variability and DNA sequences of constructs used in this study (PDF)

AUTHOR INFORMATION

Corresponding Authors

*E-mail: t.f.a.d.greef@tue.nl.

*E-mail: w.huck@science.ru.nl.

ORCID

Wilhelm T. S. Huck: 0000-0003-4222-5411

Author Contributions

§M.Y. and A.J.v.d.L. contributed equally to this work. W.T.S.H. and T.d.G. conceived and supervised the project. M.Y.,

DOI: 10.1021/acssynbio.8b00300
ACS Synth. Biol. 2018, 7, 2879−2887

A.J.v.d.L., and P.A.P. performed the experiments. M.Y., A.J.v.d.L., and B.v.S. analyzed the data. All authors contributed to writing the manuscript.

Notes

The authors declare no competing financial interest.

■ ACKNOWLEDGMENTS

We thank Frank H. T. Nelissen, Hans A. Heus and Evan Spruijt for helpful discussions and Roel Maas for his help with experiments. W.T.S.H. was supported by a TOPPUNT grant from The Netherlands Organization for Scientific Research (NWO). T.d.G was supported by the European Research Council, ERC (project no. 677313 BioCircuit) and NWO-VIDI grant from The Netherlands Organization for Scientific Research (NWO, 723.016.003), and funding from the Ministry of Education, Culture and Science (Gravity programs, 024.001.035 and 024.003.013).

■ REFERENCES

(1) Collins, J. J., Gardner, T. S., and Cantor, C. R. (2000) Construction of a genetic toggle switch in Escherichia coli. *Nature 403*, 339−342.

(2) Elowitz, M. B., and Leibler, S. (2000) A synthetic oscillatory network of transcriptional regulators. *Nature 403*, 335−8.

(3) Fung, E., Wong, W. W., Suen, J. K., Bulter, T., Lee, S.-G., and Liao, J. C. (2005) A synthetic gene − metabolic oscillator. *Nature 435*, 118−122.

(4) Stricker, J., Cookson, S., Bennett, M. R., Mather, W. H., Tsimring, L. S., and Hasty, J. (2008) A fast, robust and tunable synthetic gene oscillator. *Nature 456*, 516−9.

(5) Xie, Z., Liu, S. J., Bleris, L., and Benenson, Y. (2010) Logic integration of mRNA signals by an RNAi-based molecular computer. *Nucleic Acids Res. 38*, 2692−2701.

(6) Angelici, B., Mailand, E., Haefliger, B., and Benenson, Y. (2016) Synthetic Biology Platform for Sensing and Integrating Endogenous Transcriptional Inputs in Mammalian Cells. *Cell Rep. 16*, 2525−2537.

(7) Weber, W., Schoenmakers, R., Keller, B., Gitzinger, M., Grau, T., Daoud-El Baba, M., Sander, P., and Fussenegger, M. (2008) A synthetic mammalian gene circuit reveals antituberculosis compounds. *Proc. Natl. Acad. Sci. U. S. A. 105*, 9994−9998.

(8) Shao, J., Xue, S., Yu, G., Yu, Y., Yang, X., Bai, Y., Zhu, S., Yang, L., Yin, J., Wang, Y., Liao, S., Guo, S., Xie, M., Fussenegger, M., and Ye, H. (2017) Smartphone-controlled optogenetically engineered cells enable semiautomatic glucose homeostasis in diabetic mice. *Sci. Transl. Med. 9*, 1−14.

(9) Ro, D. K., Paradise, E. M., Quellet, M., Fisher, K. J., Newman, K. L., Ndungu, J. M., Ho, K. A., Eachus, R. A., Ham, T. S., Kirby, J., Chang, M. C. Y., Withers, S. T., Shiba, Y., Sarpong, R., and Keasling, J. D. (2006) Production of the antimalarial drug precursor artemisinic acid in engineered yeast. *Nature 440*, 940−943.

(10) Paddon, C. J., Westfall, P. J., Pitera, D. J., Benjamin, K., Fisher, K., McPhee, D., Leavell, M. D., Tai, A., Main, A., Eng, D., Polichuk, D. R., Teoh, K. H., Reed, D. W., Treynor, T., Lenihan, J., Jiang, H., Fleck, M., Bajad, S., Dang, G., Dengrove, D., Diola, D., Dorin, G., Ellens, K. W., Fickes, S., Galazzo, J., Gaucher, S. P., Geistlinger, T., Henry, R., Hepp, M., Horning, T., Iqbal, T., Kizer, L., Lieu, B., Melis, D., Moss, N., Regentin, R., Secrest, S., Tsuruta, H., Vazquez, R., Westblade, L. F., Xu, L., Yu, M., Zhang, Y., Zhao, L., Lievense, J., Covello, P. S., Keasling, J. D., Reiling, K. K., Renninger, N. S., and Newman, J. D. (2013) High-level semi-synthetic production of the potent anti-malarial artemisinin. *Nature 496*, 528−532.

(11) Borkowski, O., Ceroni, F., Stan, G. B., and Ellis, T. (2016) Overloaded and stressed: whole-cell considerations for bacterial synthetic biology. *Curr. Opin. Microbiol. 33*, 123−130.

(12) Niederholtmeyer, H., Stepanova, V., and Maerkl, S. J. (2013) Implementation of cell-free biological networks at steady state. *Proc. Natl. Acad. Sci. U. S. A. 110*, 15985−90.

(13) Sun, Z. Z., Yeung, E., Hayes, C. A., Noireaux, V., and Murray, R. M. (2014) Linear DNA for rapid prototyping of synthetic biological circuits in an escherichia coli based TX-TL cell-free system. *ACS Synth. Biol. 3*, 387−397.

(14) Shin, J., and Noireaux, V. (2010) Efficient cell-free expression with the endogenous E. coli RNA polymerase and sigma factor 70. *J. Biol. Eng. 4*, 2−10.

(15) Caschera, F., and Noireaux, V. (2014) Synthesis of 2.3 mg/mL of protein with an all Escherichia coli cell-free transcription-translation system. *Biochimie 99*, 162−168.

(16) Shin, J., and Noireaux, V. (2010) Study of messenger RNA inactivation and protein degradation in an Escherichia coli cell-free expression system. *J. Biol. Eng. 4*, 9.

(17) Iskakova, M. B., Szaflarski, W., Dreyfus, M., Remme, J., and Nierhaus, K. H. (2006) Troubleshooting coupled in vitro transcription-translation system derived from Escherichia coli cells: Synthesis of high-yield fully active proteins. *Nucleic Acids Res. 34*, e135.

(18) Stögbauer, T., Windhager, L., Zimmer, R., and Rädler, J. O. (2012) Experiment and mathematical modeling of gene expression dynamics in a cell-free system. *Integr. Biol. 4*, 494−501.

(19) Shin, J., and Noireaux, V. (2012) An E. coli Cell-free expression toolbox: Application to synthetic gene circuits and artificial cells. *ACS Synth. Biol. 1*, 29−41.

(20) Garamella, J., Marshall, R., Rustad, M., and Noireaux, V. (2016) The All E. coli TX-TL Toolbox 2.0: A Platform for Cell-Free Synthetic Biology. *ACS Synth. Biol. 5*, 344−355.

(21) Marshall, R., Maxwell, C. S., Collins, S. P., Jacobsen, T., Luo, M. L., Begemann, M. B., Gray, B. N., January, E., Singer, A., He, Y., Beisel, C. L., and Noireaux, V. (2018) Rapid and Scalable Characterization of CRISPR Technologies Using an E. coli Cell-Free Transcription-Translation System. *Mol. Cell 69*, 146−157e3.

(22) Adamala, K. P., Martin-Alarcon, D. A., Guthrie-Honea, K. R., and Boyden, E. S. (2017) Engineering genetic circuit interactions within and between synthetic minimal cells. *Nat. Chem. 9*, 431−439.

(23) Karzbrun, E., Tayar, A. M., Noireaux, V., and Bar-Ziv, R. H. (2014) Programmable on-chip DNA compartments as artificial cells. *Science (Washington, DC, U. S.) 345*, 829−832.

(24) Niederholtmeyer, H., Sun, Z. Z., Hori, Y., Yeung, E., Verpoorte, A., Murray, R. M., and Maerkl, S. J. (2015) Rapid cell-free forward engineering of novel genetic ring oscillators. *eLife 4*, 1−18.

(25) Novák, B., and Tyson, J. J. (2008) Design principles of biochemical oscillators. *Nat. Rev. Mol. Cell Biol. 9*, 981−91.

(26) O'Brien, E. L., Van Itallie, E., and Bennett, M. R. (2012) Modeling synthetic gene oscillators. *Math. Biosci. 236*, 1−15.

(27) Mooney, R. A., Darst, S. A., and Landick, R. (2005) Sigma and RNA polymerase: An on-again, off-again relationship? *Mol. Cell 20*, 335−345.

(28) Grigorova, I. L., Phleger, N. J., Mutalik, V. K., and Gross, C. A. (2006) Insights into transcriptional regulation and sigma competition from an equilibrium model of RNA polymerase binding to DNA. *Proc. Natl. Acad. Sci. U. S. A. 103*, 5332−5337.

(29) Maeda, H., Fujita, N., and Ishihama, A. (2000) Competition among seven Escherichia coli sigma subunits: relative binding affinities to the core RNA polymerase. *Nucleic Acids Res. 28*, 3497−503.

(30) Mauri, M., and Klumpp, S. (2014) A Model for Sigma Factor Competition in Bacterial Cells. *PLoS Comput. Biol. 10*, 29−34.

(31) Park, J., Dies, M., Lin, Y., Hormoz, S., Smith-Unna, S. E., Quinodoz, S., Hernández-Jiménez, M. J., Garcia-Ojalvo, J., Locke, J. C. W., and Elowitz, M. B. (2018) Molecular Time Sharing through Dynamic Pulsing in Single Cells. *Cell Syst. 6*, 216−229e15.

(32) Bervoets, I., Van Brempt, M., Van Nerom, K., Van Hove, B., Maertens, J., De Mey, M., and Charlier, D. (2018) A sigma factor toolbox for orthogonal gene expression in Escherichia coli. *Nucleic Acids Res. 46*, 2133−2144.

(33) Tayar, A. M., Karzbrun, E., Noireaux, V., and Bar-Ziv, R. H. (2017) Synchrony and pattern formation of coupled genetic

DOI: 10.1021/acssynbio.8b00300
ACS Synth. Biol. 2018, 7, 2879−2887

oscillators on a chip of artificial cells. *Proc. Natl. Acad. Sci. U. S. A. 114*, 201710620.
(34) Dunlap, J. C. (1999) Molecular bases for circadian clocks. *Cell 96*, 271−290.
(35) Raue, A., Kreutz, C., Maiwald, T., Bachmann, J., Schilling, M., Klingmüller, U., and Timmer, J. (2009) Structural and practical identifiability analysis of partially observed dynamical models by exploiting the profile likelihood. *Bioinformatics 25*, 1923−1929.
(36) Smith, R. W., van Sluijs, B., and Fleck, C. (2017) Designing synthetic networks in silico: A generalised evolutionary algorithm approach. *BMC Syst. Biol. 11*, 1−19.
(37) Sun, Z. Z., Hayes, C. A., Shin, J., Caschera, F., Murray, R. M., and Noireaux, V. (2013) Protocols for implementing an Escherichia coli based TX-TL cell-free expression system for synthetic biology. *J. Visualized Exp.*, No. e50762.
(38) Farewell, A., Kvint, K., and Nyström, T. (1998) Negative regulation by RpoS: A case of sigma factor competition. *Mol. Microbiol. 29*, 1039−1051.
(39) Rondelez, Y. (2012) Competition for catalytic resources alters biological network dynamics. *Phys. Rev. Lett. 108*, 1−5.
(40) Kim, P. M., and Tidor, B. (2003) Limitations of Quantitative Gene Regulation Models : A Case Study Limitations of Quantitative Gene Regulation Models : A Case Study. *Genome Res. 13*, 2391−2395.
(41) Purnick, P. E. M., and Weiss, R. (2009) The second wave of synthetic biology: From modules to systems. *Nat. Rev. Mol. Cell Biol. 10*, 410−422.
(42) Qian, Y., Huang, H. H., Jiménez, J. I., and Del Vecchio, D. (2017) Resource Competition Shapes the Response of Genetic Circuits. *ACS Synth. Biol. 6*, 1263−1272.
(43) Siegal-Gaskins, D., Tuza, Z. A., Kim, J., Noireaux, V., and Murray, R. M. (2014) Gene circuit performance characterization and resource usage in a cell-free "breadboard. *ACS Synth. Biol. 3*, 416−425.

DOI: 10.1021/acssynbio.8b00300
ACS Synth. Biol. 2018, 7, 2879−2887